INSTITUT DE FRANCE
Académie des sciences

Comptes Rendus

Géoscience

Sciences de la Planète

Francesco Vetere, Gianluca Iezzi, Diego Perugini and Francois Holtz

Rheological changes in melts and magmas induced by crystallization and strain rate

Volume 354, Special Issue S1 (2022), p. 227-248

Published online: 6 May 2022
Issue date: 1 December 2022

https://doi.org/10.5802/crgeos.125

Part of Special Issue: Glass, an ubiquitous material
Guest editor: Daniel Neuville (Université de Paris, Institut de physique du globe de Paris, CNRS)

Les Comptes Rendus. Géoscience — Sciences de la Planète *sont membres du Centre Mersenne pour l'édition scientifique ouverte*
www.centre-mersenne.org
e-ISSN : 1778-7025

Comptes Rendus
Géoscience — Sciences de la Planète
2022, Vol. 354, Special Issue S1, p. 227-248
https://doi.org/10.5802/crgeos.125

Glass, an ubiquitous material / *Le verre, un matériau omniprésent*

Rheological changes in melts and magmas induced by crystallization and strain rate

Francesco Vetere [*, a, b, c], **Gianluca Iezzi** [b, d], **Diego Perugini** [e] **and Francois Holtz** [c]

[a] Dipartimento di Scienze Fisiche, della Terra e dell'Ambiente (DSTA) Università di Siena 53100, Siena, Italy

[b] Dipartimento di Ingegneria & Geologia (InGeO), Università G. D'Annunzio di Chieti-Pescara, Via dei Vestini 31, 66100, Chieti, Italy

[c] Institut of Mineralogy, Leibniz Universität Hannover, Callinstrasse 3, 30167 Hannover, Germany

[d] Istituto Nazionale di Geofisica e Vulcanologia, INGV, Via di Vigna Murata 605, 00143, Roma, Italy

[e] Department of Physics and Geology, University of Perugia, Piazza Università 1, 06100 Perugia, Italy

E-mails: francesco.vetere@unisi.it (F. Vetere), g.iezzi@unich.it (G. Iezzi), diego.perugini@unipg.it (D. Perugini), f.holtz@mineralogie.uni-hannover.de (F. Holtz)

Abstract. This review highlights the rheological and phase proportions variation induced by cooling events from superliquidus temperature (melt) to subliquidus temperatures. It provides a comprehensive view of the rheological response of magmatic systems undergoing dynamic cooling and shear deformation. The two main parameters which are of importance to model the rheological properties of such crystallizing systems and which are simultaneously poorly investigated so far are crystallization and strain rates. The response to relatively high deformation rates results in shear thinning behavior in partly crystallized systems under variable shear rate and it should be considered in magmatic processes. Due to the sluggish crystallization of SiO_2-rich melts, data are mainly available for mafic systems, which does not allow a general reappraisal. An attempt to model available literature data for less evolved systems in dynamic scenarios and a comparison with MELTS algorithm approach (thermodynamic equilibrium conditions) is provided. Since there are difficulties in comparing experimental data gained using different methodologies, we focus mainly on data obtained with the concentric cylinder technique. This highlights the fact that a general experimental protocol is needed in order to compare and model viscosity data to predict the dynamic rheological evolution for volcanic rocks.

Keywords. Viscosity, Crystal nucleation and growth, Magma rheology, Cooling rate, Modelling.

Published online: 6 May 2022, Issue date: 1 December 2022

* Corresponding author.

1. Introduction

Rheological behavior of silicate melts and magmas are of high importance to understand how they form, travel, and emplace into and on the Earth's surface. A special role in the magmatic evolution is exerted by the melt/magma undercooling degree(s); it is defined as the difference between the system temperature and the temperature at which a phase saturates in the given liquid [Kirkpatrick, 1981, Giuliani et al., 2021]. From a thermodynamic point of View, the appearance of solid phases from a magma is driven by the undercooling degree. However, the nucleation and crystals growth of a mineral phase is also governed by kinetics processes [Lofgren, 1980, Dowty, 1980, Hammer, 2008, Iezzi et al., 2008, 2009, Vetere et al., 2013, 2015, Giuliani et al., 2020b,a]. The overall variation in nucleation rate spans many orders of magnitude, while growth rates variation is more limited [Swanson, 1977, Kirkpatrick, 1981, Lasaga, 1997, Cashman, 1988, Hammer and Rutherford, 2002, Zhang, 2008, Iezzi et al., 2009, Mollo and Hammer, 2017, Giuliani et al., 2020b]. For a similar bulk magmatic composition, a low nucleation rate produces few crystals that will became large, while a high nucleation rate will result in a large number of tiny crystals [Hammer, 2008, Iezzi et al., 2009, Higgins, 2006, Mollo and Hammer, 2017]. Nucleation is favored in silicate liquids with a high chemical diffusion, i.e., poor in SiO_2 and rich in H_2O, whereas SiO_2- and H_2O-poor liquids are reluctant to nucleate and prone to vitrify [Iezzi et al., 2009, Vetere et al., 2015].

Nucleation and crystallization processes have profound implications for the rheology of magmas and lavas, which depends on the volumetric amount of solid phases as well as on their size and shape [Gonnermann and Manga, 2007]. Hence, a clear knowledge of nucleation and crystallization processes driven by solidification, either by cooling or by degassing-induced depressurization, is the key to understand magma rheology and its evolution before turning into a solid rock.

The eruptive style of volcanoes is strongly affected by magma viscoelastic properties [Dingwell, 1996, Gonnermann and Manga, 2007, Cassidy et al., 2018, and reference therein] and, as shown by Petrelli et al. [2018], their associated timescales. Indeed, the P–T–fO_2 path(s) for a starting magmatic composition (X) governs its solidification behavior and rheological pathway [Lanzafame et al., 2013, 2017].

Crystallization under kinetic conditions imposed by $\Delta T/\Delta t$ and/or $\Delta P/\Delta t$ was experimentally studied and investigated mainly for mafic compositions so far [Arzilli et al., 2019, Polacci et al., 2018, Hammer, 2008, Conte et al., 2006, Fiege et al., 2015, and reference therein], while highly evolved melts are harsher to experimental investigation (time consuming), especially in a dry context [Vetere et al., 2013, 2015]. Nowadays, it is recognized that disequilibrium conditions often occur in natural processes [Kolzenburg et al., 2018, Vetere et al., 2019, 2021, and reference therein]. Moreover, ambiguities persist in our understanding of the interplay between crystal nucleation and growth on magma rheological variation (bulk viscosity and density) as it evolves from liquidus temperature down to the glass transition temperature, T_g. The cooling rate and degassing rate induced by depressurization of magmatic batches influence textural, petrological, and geochemical features, as well as volcanic behavior, i.e., from mildly lava effusion to violent explosive paroxysm [Armienti, 2008, Hammer, 2008, Applegarth et al., 2013, Shea and Hammer, 2013, Fiege et al., 2015, Mollo and Hammer, 2017, Arzilli et al., 2019, and references therein].

Due to the changes in residual melt chemistry and solid phase growth (as melt solidifies below the liquidus temperature, T_L), it is expected that properties such as the apparent viscosity and density will vary, with significant impact on the magma's ability to move [Giuliani et al., 2021]. To have an overview of this natural scenario and because of the paucity of direct field data [Chevrel et al., 2019, 2018, 2015], experimental approach is of paramount importance to further understand how magma behaves as it moves into and on the Earth.

In this review, after a general discussion on the nucleation and growth of minerals in silicate melts and magmas and on the general and most used laws and models governing magma rheology, we will focus both on recent experimental data on natural/synthetic systems and numerical approach with the aim to examine equilibrium versus disequilibrium conditions on the solidification of mafic compositions and its impact on rheological behavior. Specifically, we will constrain and model the rheological changes induced by cooling and also by shear stresses. Results point to the complex

interactions between crystallization processes and rheological behavior as the key for understanding how magmas behave in natural systems. We will also emphasize the possible future experimental approaches in order to shed new light on these important natural processes that could be applicable to solidification induced by depressurization for volatile-rich magmas.

2. The state of the art

Petrological processes and scenarios are interpreted and reconstructed mainly by studying crystal-chemical attributes of phases [Giuliani et al., 2021, 2022]. This approach commonly assumes thermodynamic equilibrium between magmatic liquid and their mineral/volatile phases. From thermodynamically derived laws, intensive variables of magmatic systems can be obtained by crystal-chemistry of minerals and coexisting liquids, such as to track evolution of magmas [e.g., Putirka, 2008, and references therein]. However, we now have clear evidence of disequilibrium features in both intrusive and especially volcanic rocks [e.g., De Paolo and Getty, 1996, Roselle et al., 1997, Müller et al., 2004, Nabelek, 2007, Baker, 2008, Mollo and Hammer, 2017, Giuliani et al., 2021]. Hence, the scientific community is aware that compositional changes of minerals in volcanic rocks are not necessarily related to equilibrium conditions, but rather and frequently to a disequilibrium state [e.g., Baker and Grove, 1985, Hammer, 2006, 2008, Iezzi et al., 2008, 2011, Del Gaudio et al., 2010, Mollo et al., 2010, 2011b,a]. For a bulk chemical composition of a magmatic batch, the increase of undercooling degree and deformation rate (i.e., stretching and folding mechanisms) progressively induces and facilitates nucleation and crystallization processes [Swanson and Ottino, 1990, Perugini et al., 2008, Rossi et al., 2019, Tripoli et al., 2019]; in turn, they strongly affect rheological behavior of magmas that eventually rise from depth and emplace on the Earth's surface. Deformations occurring in dynamic magmas enhance the nucleation and crystal growth; the movement of a magma furnishes continuous and fresh "*feeding ingredients*" around early formed crystals [Vetere et al., 2020, Vetere and Holtz, 2020] when compared to a static condition. Also, in order to better understand the rheology of complex systems, another important aspect is related to the delay in crystal nucleation and growth that became progressively higher at low undercooling degree, i.e., close to liquidus temperature [Rusiecka et al., 2020, Giuliani et al., 2020a].

Rheology is defined as the science studying the deformation of materials under well-defined conditions. As defined in Mezner [2014], the term rheology (i.e., the flow science) derives from the Greek word "*rhein*" that is equivalent to the word "*flow*." When applied to volcanology, the rheology of magmas essentially studies melt or magma flows as they are subjected to different stress, in magma chambers, along the way to the surface or when flowing on the Earth's surface or other planetary surface (Mercury or Mars, for example). Starting from the definition of magma, it also implies that the rheological behavior depends mainly on phases present in a system (fluid ± crystals ± exsolved and dissolved volatiles), which depend on a variety of parameters such as pressure, temperature, and fO_2 for a well-defined chemical system. In addition, it is now clear that such a behavior can change if phases are subjected to certain stress [e.g., shear rate dependence; Vetere and Holtz, 2020 and reference therein]. In the conventional description of rheological data, in order to parameterize any suspension, there is a need to clearly define the relationship between the imposed shear stress (σ in Pa) and the shear strain-rate ($\dot{\gamma}$ in s^{-1}; i.e., deformation rate). This relationship can be used to characterize the flow behavior and related flow curve. The flow regime is usually defined as Newtonian when there is a simple proportionality between stress and strain:

$$\sigma = \eta \cdot \dot{\gamma}, \tag{1}$$

where η (in Pa·s) is the Newtonian viscosity (Figure 1).

However, in multiphase and complex systems, such as magma, deviation from Newtonian behavior is observed and shear stress is not simply proportional to strain rate and the following cases are common: (1) a minimum stress is required before viscous flow initiates (also called the Bingham regime) or (2) both the above behaviors are combined, which is expressed by the Herschel–Bulkley model [Herschel and Bulkley, 1926]:

$$\sigma = \tau_y + K\dot{\gamma}^n, \tag{2}$$

where τ_y is the yield stress, K is the flow consistency, and n the flow index (details are shown in Figure 1) [Herschel and Bulkley, 1926, Wildemuth and

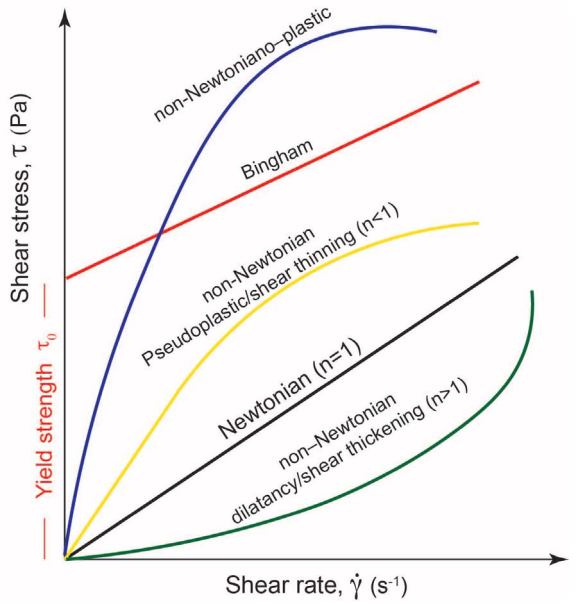

Figure 1. Newtonian and non-Newtonian behavior [Lenk, 1967]. τ_y is the yield stress that is to be overcome in order to initiate flow; n is the flow index describing the degree of non-Newtonian behavior. For Newtonian materials $\tau_y = 0$, $n = 1$, and the flow consistency $K = \eta$; shear-thickening and shear-thinning materials are defined by $n > 1$ and $n < 1$, respectively.

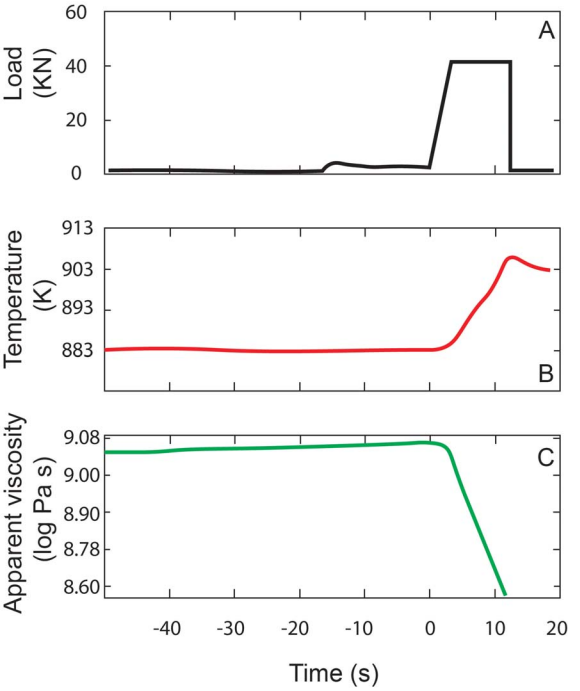

Figure 2. Results of viscosity measurements using the Parallel plate viscometry on NIST-certified starting glass as reported in Cordonnier et al. [2012]. (A) Load applied to the sample; (B) Due to the applied load (when it is high enough), the temperature in the sample increases; (C) As temperature increases (B) viscosity drops. This viscosity drop is explained from the temperature increase and can also be predicted by the Vogel–Tamann–Fulcher equation [Hess et al., 2007].

Williams, 1984, Mueller et al., 2010, Mader et al., 2013, Moitra and Gonnermann, 2015].

The onset of **non-Newtonian rheology** in silicate melts has been investigated by Webb and Dingwell [1990a,b] using fiber elongation techniques. The chosen melt compositions were a high silica rhyolite, an andesite, a tholeiitic basalt, and a nephelinite. Viscosity was determined as the ratio of the applied tensile stress to the observed strain rate. As reported by the authors, "*before experiments, each fiber was initially annealed at a temperature for a period of* 10^4 *s. This equilibration time is greater than both the shear and volume relaxation times of a melt with* $\eta v = \eta s = 10^{12}$ *Pa·s and* G_∞ *(shear modulus)* $\approx K_\infty$ *(bulk modulus) 10 GPa* ($t_V = t_S = 100$ *s).*" However, the measurements had no in situ monitoring of the sample temperature and did not consider viscous heating effects. Figure 2 illustrates the apparent viscosity reduction due to viscous heating effect. As reported by Cordonnier et al. [2012], "*fluids with a temperature-dependent viscosity are affected by viscous heating once this heat source overcomes the heat loss (i.e., heat transfer by conduction, convection, and/or radiation).*" This effect, despite increasing shear rates, will move magmas away from the glass transition [Gonnermann and Manga, 2007]. Yue and Bruckner [1996] have re-analyzed the fiber elongation observations and formulated a correction for the strain-rate dependence of viscosity that includes viscous heating effects explicitly. The question as to whether viscous heating may have had a measurable effect on previous determinations of the onset of non-Newtonian viscosity remains unsolved.

Because magmatic suspensions are strain rate dependent, thus sensitive to the applied shear stress,

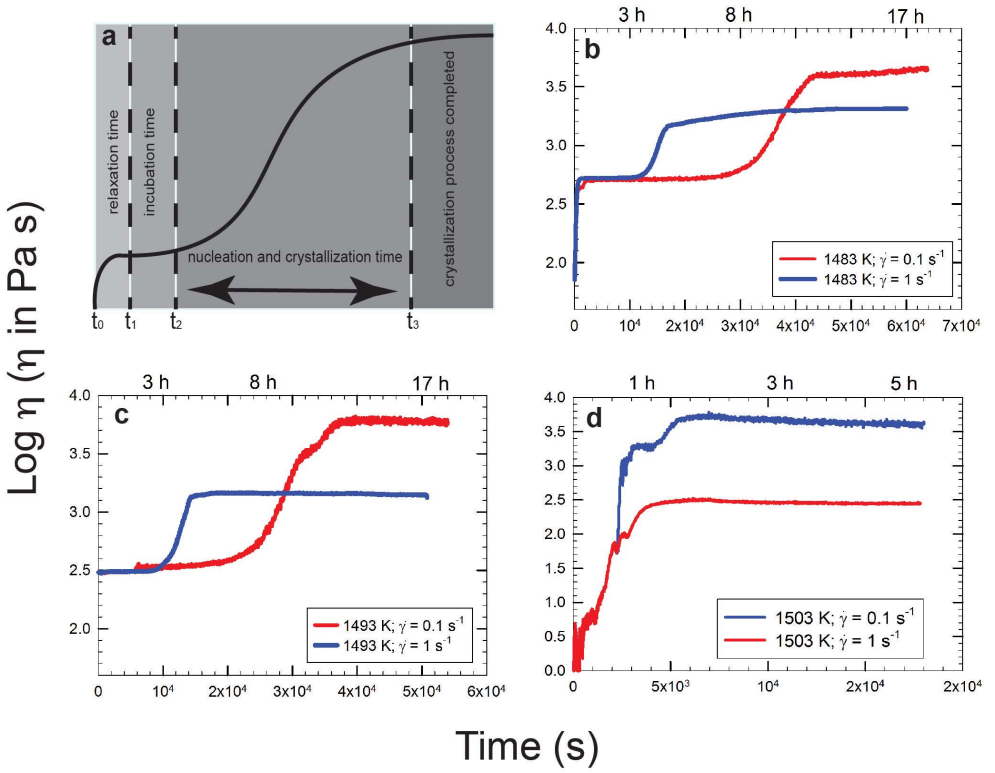

Figure 3. Note: Apparent viscosity variation versus time; (a) redraw from Vona et al. [2011] while (b–d) are redrawn from Vetere and Holtz [2020] and refer to (b) andesite from Calbuco 2015 eruptions, (c) Etna basalt from 122 A.C eruption, and (d) pyroxenite from Theo's Flow which is a proxy for Martian lava flow samples. Blue and red curves refer to experiments performed at shear rate of 1 and 0.1 s^{-1}, respectively. Note the shear-thinning behavior (apparent viscosity decreases as shear rate increases) with nucleation and crystallization processes related to the applied deformation rates (see text for details).

it is common to define the relative viscosity η_r as:

$$\eta_r = \frac{\eta_{\text{app}}}{\eta_l}, \tag{3}$$

where η_{app} defines the ratio of a given stress to a given strain-rate, meaning that the obtained results are only valid for specific deformation conditions and, thus, vary with strain-rate, and η_l is the liquid viscosity. Particular consideration must be given to the fact that multiphase suspension deforms when subjected to stress; for magmas the most common deformation relates to shear, while other types of deformation like oscillatory, tensile, or compressive behaviors are limited or even absent [details are given in Dingwell, 1995, Dingwell and Webb, 1989, Webb and Dingwell, 1990a,b]. It is intuitive that the viscosity of a suspension is different from the viscosity of the liquid component. Moreover, the solid phases in suspensions can vary in terms of their volume, size, and shape, and this can drastically affect the rheology of the system [Kerr and Lister, 1991, Mueller et al., 2010, Pistone et al., 2016, Arzilli et al., 2019, Kolzenburg et al., 2020, and reference therein]. As an example, prolate or oblate particles in magma could be present and can act as a different opponent to the applied shear stress and, as consequence, to the flow ability (e.g., if particles' major axes are aligned to flow direction, their influence on flow velocity is minor compared with the opposed cases as with particles' major axes orthogonal to the flow).

Vona et al. [2011] provided a methodology to follow for the evolution of the apparent viscosity as crystallization processes proceed. Figure 3a shows an *S-shape* curve where relaxing, incubation,

nucleation times, and crystallization processes with a final plateau (denoting the end of the crystallization process) are highlighted. This cartoon is confirmed by experimental data for different compositions (as those presented in the following paragraph). The steepness of the curve is related to the response of the melt when temperature is below the liquidus. In other words, the curve shows the time that is needed for a melt to relax and eventually to start to nucleate a solid phase. As expected, very fluid systems react much faster than more viscous ones and this is clearly evidenced in Figures 3b–d where three different melts with compositions varying from andesite (typical intermediate composition between basalt and rhyolite) to basalt and to pyroxenite (an ultramafic igneous rock consisting essentially of minerals of the pyroxene group) are compared. Obviously, considering the red curves in Figure 3 (e.g., experiments performed at shear rate = 0.1 s^{-1}) the most depolymerized pyroxenite composition (Figure 3d) reacts faster (ca. 1800 s) when compared to basalt (ca. 2×10^4 s; Figure 3c) and basalt reacts faster when compared to andesitic composition (ca. 3×10^4 s; Figure 3b).

The last consideration on partly crystallized system concerns the approach to the so-called maximum packing fraction (Φ_m) where the viscosity of a suspension (thus, the ability of a melt plus crystal system to flow) tends to infinity and the transition from viscous to elastic behavior might occur. Φ_m depends on particle sizes, shapes, and distributions and its value during a flow may change due to possible crystal alignment along the flow directions [see the concept of rheological critical melt percentage, RCMP as discussed in Arzi, 1978 and reviewed by Rosenberg and Handy, 2005].

3. Investigated compositions

The bulk compositions reconsidered and used in this review are reported in Figure 4 (Supplementary Appendix 1), on which both kinetics-controlled crystallization events, rheological test, and/or numerical modeling have been performed.

A first compositional dataset comprises rheological experimental data in which shear stress vary at isothermal conditions, ideally at a fixed undercooling degree [Morrison et al., 2020, Sehlke and Whittington, 2020, 2015, Vetere and Holtz, 2020, Vetere et al., 2020, 2017, Campagnola et al., 2016, Sehlke et al., 2014, Vona et al., 2011, Ishibashi, 2009, Ishibashi and Sato, 2007]. However, it is important to state that magmatic suspensions are complex chemical systems, where crystallizing phases have different compositions from the parental liquids [Iezzi et al., 2020]. Thereby, also at isothermal condition, the crystallization trough time determines a change in composition of both crystalline and liquid phases. The second dataset, although very limited, comprises rheological data derived upon shearing and cooling events acting on silicate liquids, and represent the closest to natural scenarios [Vetere et al., 2019, Kolzenburg et al., 2020, 2019, 2018].

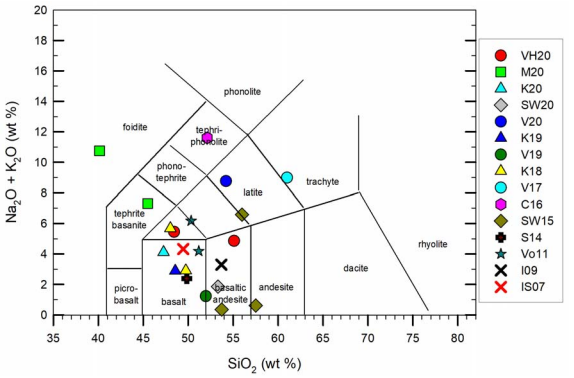

Figure 4. Note: Total alkalis versus silica diagram for the investigated starting compositions. VH20 refers to Vetere and Holtz [2020]; V20, 19 and 17 refer to Vetere et al. [2020, 2019, 2017, respectively]; M20 refers to Morrison et al. [2020]; K20, 19 and 18 as in Kolzenburg et al. [2020, 2019, 2018, respectively]; SW20 and 15 refer to Sehlke and Whittington [2020, 2015]; C16 refers to Campagnola et al. [2016]; S14 refers to Sehlke et al. [2014]; Vo11 refers to Vona et al. [2011]; I09 to Ishibashi [2009] and IS07 to Ishibashi and Sato [2007].

These two experimental datasets were obtained with the identical methodology (i.e., concentric cylinder) and mirrors a viscosity range of 10^1–10^6 Pa·s, thus, partly crystallized silicate melts, where the magma dynamic regime is dictated by crystallinity (Φ). Usually this regime varies from dilute (where Φ varies between 0.05 and 0.25 and particles have low to moderate interaction mainly depending on the particle aspect ratio) to semi dilute regime

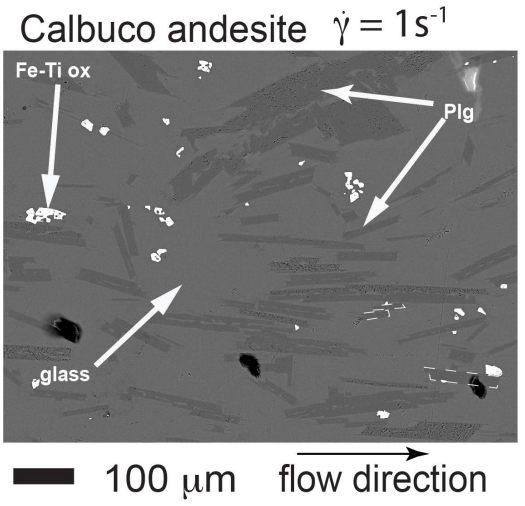

Figure 5. Concentric cylinder experimental results on Calbuco andesite at shear rate of 1 s^{-1} and temperature of 1483 K as in Vetere and Holtz [2020]. Phases are Fe–Ti oxides, plagioclase (plg), and glass. Note the plagioclase (plg) alignment along the flow direction.

(~0.25⟨Φ⟩~0.6) where particles strongly interact with each other with a possible alignment with the flow direction [Figure 5; Hoover et al., 2001, Saar et al., 2001, Vetere and Holtz, 2020]. Both regimes define non-Newtonian systems with shear thinning behavior (small or strong, depending on Φ) with a possible evolution of the apparent yield stress (Figure 1). Those data reveal the importance of dynamic applied to silicate melts under cooling as will be discussed below.

4. Numerical simulation

AlphaMELTS code was used to track the phase evolution path for compositions presented in Figure 4 as temperature cools from the liquidus to subliquidus conditions. The alphaMELTS (V. 1.9) software provide a simple text-based interface to subroutine versions of the algorithms MELTS, pMELTS, and pHMELTS [Asimow and Ghiorso, 1998, Smith and Asimow, 2005, Ghiorso et al., 2002, Ghiorso and Sack, 1995]. Suitable for multi-component systems, it allows to calculate equilibrium assemblages along a thermodynamic path set by the user (for details on the software, see the following address: http://melts.ofm-research.org/ and https://magmasource.caltech.edu/forum/).

The evolution of residual melt compositions is reported in Figure 6a and the evolution of melt proportion versus temperature is shown in Figure 6b (as vol%). In both cases, a direct comparison with literature data is provided. The calculated liquidus temperature are also available in Supplementary Appendix 1 for all the studied compositions. In general, it shows progressively lower values as the chemistry of the systems evolves to more silicic ones (higher SiO_2 content), as expected, to equilibrium conditions for the modeled melts. The evolution of SiO_2 predicted in Figure 6a for samples I09, Vo11Stromboli, and Vo11Etna, as for sample M20NYI and SW15NVP–Na, shows higher values than experimental data, while the opposite is observed for sample S14, M20NYA, and, in both cases, the differences become important at lower temperatures. In general, predictions of the Al_2O_3 evolutions are more accurate as those for CaO and MgO oxides, while FeO^{tot} is overestimated for M20NYA, C16 and underestimated for Vo11Stromboli, SW15NVP, and M20NYI samples, respectively. The difference between experimental data and data predicted by alphaMELTS are particularly large for M20NYI and M20NYA compositions. As reported by Morrison et al. [2020], this is related to differences in oxygen fugacities (experimental data are obtained at more reduced conditions). Thus, we will focus only on rheological data for these compositions. The observed differences can be attributed to two aspects: (i) the inherited accuracy of the thermodynamic calculations and (ii) the occurrence of disequilibrium conditions experienced by the analyzed run-products (Figure 6a).

Experimental and thermodynamic calculations show that melt fraction decreases with temperature, as expected. In general, the very low effect of temperature on crystallinity predicted by to alphaMELTS 1.9 in the high temperature range is not reproduced by the experimental data (in particular, for M20NYA, V17, C16, SW15NVP–Na, SW15_EB, S14, and I09 compositions). In most cases, the volume of residual melt is much lower that the predicted volumes and the liquidus temperatures extrapolated from the experimental data are lower than predicted liquidus temperatures. As a result, the effect of temperature on the crystallinity in the experimental products is more

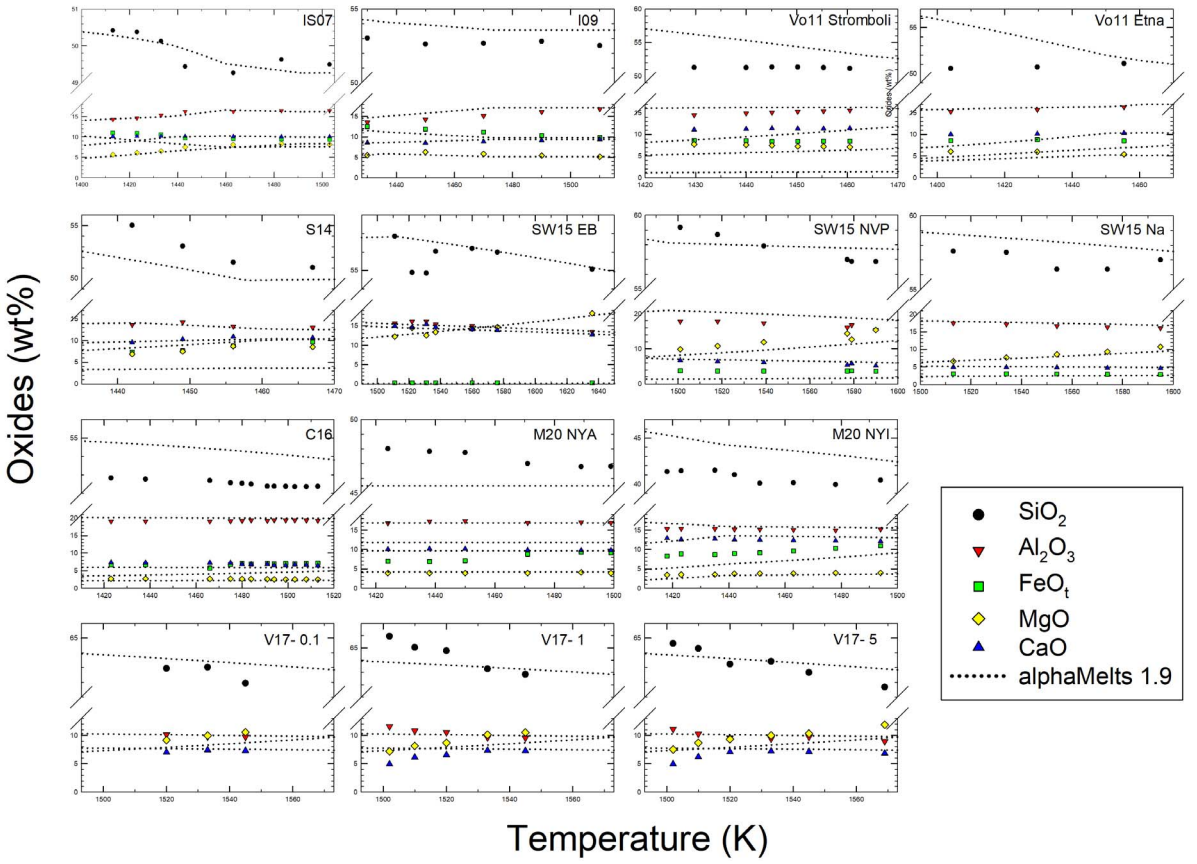

Figure 6a. SiO_2, Al_2O_3, FeOt, MgO, and CaO evolution of melts with temperature as systems cool down starting from liquidus temperatures. Symbols refer to experimental data while dotted lines refer to prediction obtained by using alphaMELTS 1.9. The label on each plot refers to chemical compositions as those reported in Figure 4.

pronounced than predicted (see also Figure 6d with the crystallinity of the individual experiments).

The composition of solid phases was compiled from the literature data and are reported in Figure 6c(A–C). The compositions of plagioclase (plg), pyroxene (px), and olivine (ol) that crystallized in the experiments are compared to predicted compositions with alphaMELTS 1.9. Predicted and experimental compositions are in general good agreement. This indicates that alphaMELTS 1.9 is successful in predicting equilibrium mineral compositions but that the prediction of phase proportions is more problematic, which may be due to calibration of the model from static experiments. Applying a shear stress to crystallization experiments is expected to promote the crystallization and reduce the delay time preceding nucleation [Rusiecka et al., 2020, Vetere et al., 2021]. Thus, the possible mechanisms to explain this difference in crystallinity might be related to the continuous stirring of the melts at high shear rate in dynamic experiments which is bringing the necessary "*feed growth ingredients*" *(elements necessary to build a crystalline structure)* close to individual crystal surfaces and which facilitates crystal growth (see below).

5. Modeling experimental data by varying shear rate and crystal content

Due to the intrinsic difficulties in performing experiments, the available experimental dataset on crystallization processes under dynamic conditions are

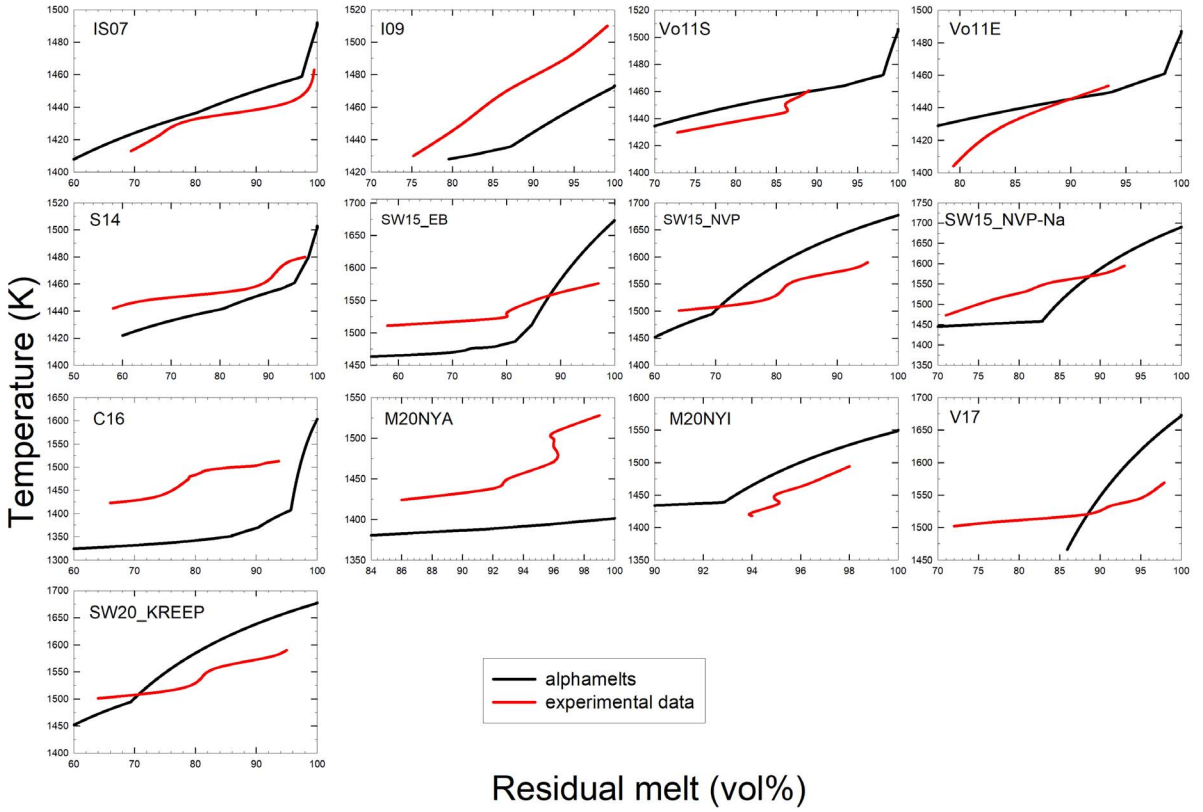

Figure 6b. Comparison of the volume of residual melt (vol%) derived from modeling and experimental data. The label in each plot corresponds to the sample numbers provided in Figures 4 and 6a. Red curves refer to experimental data while black ones are those derived from alphaMELTS 1.9 results. The red curves fitted through the experimental data sometimes show S-shapes because the curves were drawn to fit exactly the determined melt fractions. However, such a behavior is not realistic and reflects the large uncertainty in the determination of melt/crystals ratio. Data refer to ambient pressure.

still relatively scarce, as aforementioned. Moreover, the paucity of experimental data on more evolved systems is resulting from the limitations of the experimental technique (Figures 6a–6d). In particular, the range of viscosity that can be investigated with the most common apparatus to reach high stress and higher viscosity values (e.g., $\eta > 10^6$ Pa·s) does not cover that of silicic melts at moderate temperature and even with low amounts of crystals. We collected 415 literature experimental viscosity data (see Supplementary Appendices 1 and 2) on different mafic to intermediate compositions at different temperature, shear rate, volume of crystals, and 2D aspect ratio. All data were obtained with the identical methodology by using concentric cylinder apparatus and the majority show a decrease in the apparent viscosity (at isothermal conditions) as deformation rate increases, pointing to the well-known effect of shear thinning as discussed above.

Apart from viscosity data, one general outcome for most of the investigated systems is that increasing of the strain rate promotes a fast crystal growth rate. Experiments with dynamic crystallization show that only ca. 6000 s are necessary to produce ca. 22 area % of crystals having plagioclase crystal lengths of ca. 300 mm, mirroring a growth rate value of 5×10^{-6} cm/s [Vetere and Holtz, 2020], much faster than those reported in literature [i.e., 10^{-8}–10^{-9} cm/s; Pupier et al., 2008].

Considering that water and other volatiles affect the rheology of silicate melts [Fiege et al., 2015, and reference therein], the crystals' growth rate might

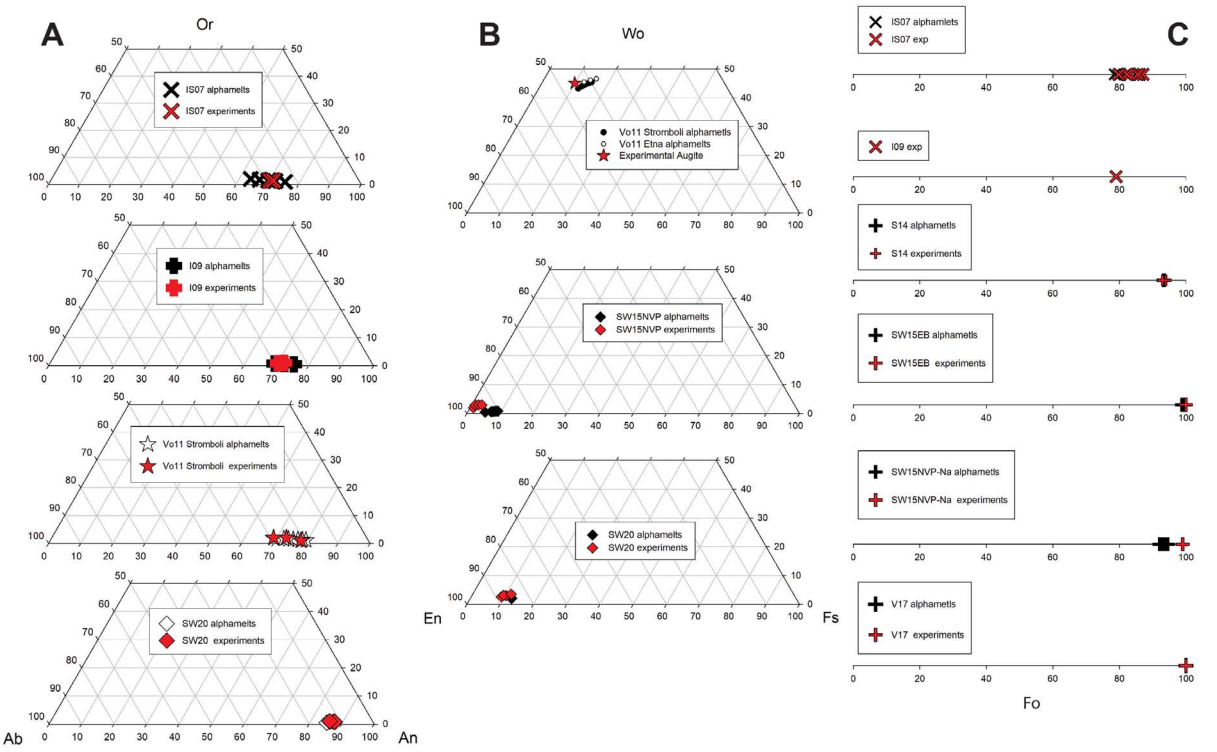

Figure 6c. (A) Plagioclase, (B) pyroxene, and (C) olivine compositions for some of the magmatic systems studied. Note the similar compositional range of experimental data and modeling.

also be dependent on strain rates in dynamic hydrous magmas. Literature provides different general models able to reproduce apparent or relative viscosity behaviors as a function of crystal content, shear rate, and aspect ratio of the solid phases. Most of them use melt viscosity in order to retrieve the relative viscosity of the suspensions (melt + crystals; see (3)), adopting general viscosity models such as proposed by Hui and Zhang [2007] or Giordano et al. [2008]. A list of the most used models is provided in Table 1.

Figure 7 provides an overview of the relative viscosity data and some of the models provided in Table 1 are plotted for comparison. All the experimental data processed at different deformation rates show a shear thinning behavior (note identical symbols with same crystal content but different η_r in Figure 7) and relative viscosity differences increase with increasing the gap between low and high shear rate. For example, Sehlke and Whittington [2015] show that NVP–Na viscosity vary from 7500 to 1500 Pa·s as shear rate vary from 0.01 to 5 s^{-1} at 1473 K with crystal content 29 vol%. Vetere et al. [2017] show a decrease of η_{app} from ca. 10200 to 1100 Pa·s at 1502 K and ca. 28 vol% of crystal as shear rate vary from 0.1 to 5 s^{-1} in synthetic silicate melt compositions analogue for Mercury (for details, please refer to Supplementary Appendix 2).

None of the models presented here are successful for predicting the whole experimental dataset. Reasons reside on the different parameters used for modeling. For example, the fact that Φ_m can vary during deformation due to possible particle alignment will obviously change the rheological behavior. And this, up to now, is not predictable. Also, the use of image analysis to retrieve solid phase proportions can lead to some uncertainties and a statistically representative dataset of BSEs images selected along different orientations of the investigated sample is necessary. Thus, when using few BSEs images, AS (AS = crystals long axis/short axis), and the average volume proportions could be influenced by the

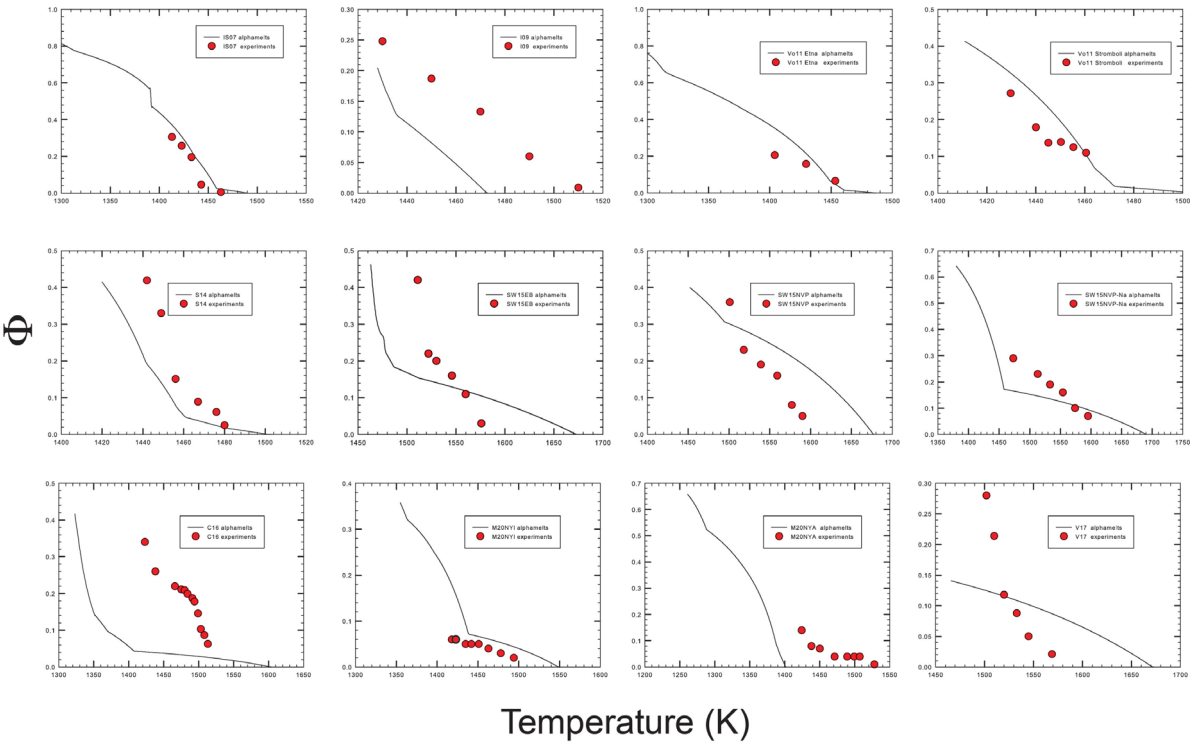

Figure 6d. Crystallinity versus temperature for the compositions reported in Figure 4.

orientation of the 2D section in a sample with a strong 3D crystal fabric [Lanzafame et al., 2017]. Ideally, analytical data based on tomographic approaches [Polacci et al., 2018, Arzilli et al., 2019] would give the solution to this problem but, up to now, especially when using concentric cylinder apparatus, it is highly difficult and techniques need improvements. Figure 7 shows also that it is possible to modify some of the parameters used in an equation in order to get a best fit with experimental data. This is the case, for instance, for the model proposed by Krieger and Dougherty [1959] which could better reproduce experimental data by varying the parameter B and Φ_m as done in Figure 7B and Table 1. However, a more exhaustive rheological model has to engulf rheological transitions from a low viscosity, where flow regime is mainly those of the suspending liquids to a high viscosity regime, where parameters such as particle shape, orientation, and volume dominate.

We performed diverse test on the dataset provided in Supplementary Appendix 2 for constraining a possible comprehensive apparent/relative viscosity model. The best solution was given by a polynomial approach, although it doesn't provide excellent results. We propose an empirical approach to retrieve the apparent viscosity from (1) shear rate and volume of solid phases or (2) AS and volume of crystals in silicate melt suspensions. Results are based on the 415 experimental data presented in Supplementary Appendix 2, interpolated by a simple polynomial approach able to build a 3D surface on which log viscosity, shear rate, and volume of crystals in one case and log viscosity, AS, and volume of crystals in the other case are taken into account (Figure 8). The apparent viscosity can be estimated using the following expressions:

$$\log\eta_{\text{app}} = a + b\cdot\ln\dot{\gamma} + c\cdot\Phi + \mathrm{d}\cdot(\ln\dot{\gamma})^2 + e\cdot\Phi^2 + f\cdot\Phi\cdot\ln\dot{\gamma} \tag{4}$$

and

$$\log\eta_{\text{app}} = a + \frac{b}{\ln \text{AS}} + \frac{c}{\text{AS}^{1.5}}\Phi + \mathrm{d}\cdot\exp(-\text{AS}) + e\cdot\Phi\cdot\ln\Phi, \tag{5}$$

Table 1. Most common relative viscosity models

	Model	Literature reference
1	$\eta_r = (1 + B\phi)$	Einstein [1906]; Dilute system ($\Phi < 0.25$) $B = 2.5$
2	$\eta_r = 1 + B\Phi + B_1\Phi^2$	Guth and Gold [1938]; Dilute system ($\Phi < 0.25$) and spherical particles $B = 2.5$, $B_1 = 14.1$
3	$\eta_r = \left(1 + \frac{1.25\Phi}{1-\frac{\Phi}{\Phi_m}}\right)^{-2}$	Eilers [1941, 1943]
4	$\eta_r = e^{\frac{B\Phi}{1-\alpha\Phi}}$	Vand [1948]
5	$\eta_r = 1 - \alpha\Phi^{-B}$	Roscoe [1952]; $\alpha = 0.135$, $B = 2.5$
6	$\eta_r = \left(1 - \frac{\Phi}{\Phi_m}\right)^{-2}$	Maron and Pierce [1956]
7	$\eta_r = \left(1 - \frac{\phi}{\phi_m}\right)^{-B\phi_m}$	Krieger and Dougherty [1959]
8	$\eta_r = \left(1 - \frac{\phi}{\phi_m}\right)^{-B\phi_m}$	Krieger and Dougherty [1959]; $B = 2.5$ for spherical particles; for elongated particles B could be modified
9	$\eta_r = \exp\left\{\left[\left(2.5 + \frac{\phi}{\phi_m - \phi}\right)^{\alpha}\right] \cdot \frac{\phi}{\phi_m}\right\}$	Gay et al. [1969]; $\alpha = 0.48$
10	$\eta_r = \left(1 - \alpha\frac{\frac{\phi}{\phi_m}}{1-\frac{\phi}{\phi_m}}\right)^2$	Chong et al. [1971]; $\alpha = 0.75$
11	$\eta_r = \frac{1}{\left(1-\frac{\Phi}{\Phi_m}\right)^{\Phi_m}}$	Wildemuth and Williams [1984]
12	$\eta_r = 1 + \frac{3\pi}{8}\frac{\beta}{\beta+1}\left[\frac{3+4.5\beta+\beta^2}{\beta+1} - 3\left(1-\frac{1}{\beta}\right)\ln(\beta+1)\right]$	Shapiro and Probstein [1992]; $\beta = \frac{\left(\frac{\phi}{\phi_m}\right)^{\frac{1}{3}}}{1-\left(\frac{\phi}{\phi_m}\right)^{\frac{1}{3}}}$
13	$\eta_r = \frac{1+\varphi^{\delta}}{\left\{1-\alpha\cdot\mathrm{erf}\left[\left(\frac{\sqrt{\pi}}{2\alpha}\cdot\varphi\right)\left(1+\varphi^{\dot{\gamma}}\right)\right]\right\}^{B\Phi_m}}$	Costa [2005]; $\varphi = \frac{\phi}{\phi_m}$
14	$\phi_m = 0.066499\tanh(0.913424)\log(\dot{\gamma}) + 3.850623 + 0.591806$ $\delta = -6.301095\tanh[(0.818496)\log(\dot{\gamma})(0.818496)\log(\dot{\gamma}) + 2.86] + 7.462405$ $\alpha = -0.000378\tanh[(1.148101)\log(\dot{\gamma}) + 3.92] + 0.999572$ $\gamma = 3.987815\tanh[(0.8908)\log(\dot{\gamma}) + 3.24] + 5.099645$	Caricchi et al. [2007] on Costa [2005] with variable strain rate

(continued on next page)

Table 1. (continued)

	Model	Literature reference
15	$\eta_r = \left(\frac{1-\varphi^\delta}{[1-F(\varphi\varepsilon\gamma)]^{B\Phi_m}}\right)^{-B\Phi_m}$ where: $F = (1-\xi)\cdot\mathrm{erf}\left[\frac{\sqrt{\pi}}{2(1-\xi)}\varphi(1+\varphi^\delta)\right]$ and $\eta_* = \eta(\Phi_m) = 2\left[1-(1-\xi)\mathrm{erf}\left(\frac{\sqrt{\pi}}{(1-\xi)}\right)\right]^{-B\Phi_m}$	Costa et al. [2009]; $\varphi = \frac{\phi}{\phi_m}$
16	$\log(\eta_r) = (-0.06\exp(6\Phi))\log\left(\frac{\tau}{\tau_{\mathrm{crit}}}\right)$	Cordonnier et al. [2009]; σ is the differential stress, σ_{crit} is the limiting stress (10^9 Pa), and $(0.06\exp(6*\phi))$ is the crystal stress dependency relation with ϕ the crystal fraction.
17	$\eta_r = \left(1-\frac{\Phi}{\Phi_m}\right)^{-\alpha\Phi_m\left[1+\beta\ln(1-\frac{\Phi}{\Phi_m})\ln\dot{\gamma}\right]}$	Ishibashi [2009]
18	$\eta_r = \left(1-\frac{\Phi}{\Phi_m}\right)^{-2[1-\alpha\log(\dot{\gamma})]}$	Vona et al. [2011]
19	$\eta_r = \left(1-\frac{\Phi}{\Phi_m}\right)^{-\alpha}$	Moitra and Gonnermann [2015]; $\alpha = 1.92$
20	$\eta_r = \left(1-\frac{\Phi_m-\Phi}{\Phi_m(1-\Phi)}\right)^{-\frac{2.5\Phi_m}{1-\Phi_m}}$	Faroughi and Huber [2015]
21	$\eta_r = \eta_{r(\max)}^{\frac{1-\exp(-k\Phi^n)}{1-\exp(-k)}}$	Liu et al. [2017]; $\eta_{r(\max)}$ is value for $\Phi = 1$. k and n are adjustable parameters

Please refer to the provided literature for details.

where η_{app} is the apparent viscosity, γ the shear rate, Φ the crystal content (vol%), and AS the crystal's aspect ratio. The fixed parameters for (4) are $a = 1.917$, $b = -0.034$, $c = 9.258$, $d = -0.032$, $e = -14.958$, and $f = -0.737$. The parameters for (5) are $a = 1.419$, $b = 0.313$, $c = -5.952$, $d = 10.499$, and $e = -6.481$. These parameters were obtained by non-linear regressions giving Root Mean Square Error (RMSE) of 0.316 and 0.319 and Mean Absolute Error (MAE) of 0.257 and 0.255 for (4) and (5), respectively. The comparison of the predicted η_{app} from (4) and (5) with experimental data is shown in Figure 9A and B, respectively.

6. The effect of shear rate, crystal content, and cooling rates

The concomitant effect of shear rate and cooling on crystallinity and rheology can be retrieved from experimental data at one atmosphere pressure, mainly obtained for mafic composition. However, the rheology of systems crystallizing as a result of degassing-induced decompression as a function of decompression-rate and shear rate was never investigated experimentally. Such experiments would simulate the nearest approach to geological relevant conditions, specifically the ascent of magmas in conduits and dikes.

Vetere et al. [2020, 2019] and Kolzenburg et al. [2020, 2019, 2018, 2017] have performed experiments at one atmosphere pressure. Due to the progressive increase in crystallinity with time during cooling (contrasting to the classical isothermal viscosity experiments presented in paragraphs 4 and 5), the apparent viscosity will never reach a steady value because of the non-equilibrium conditions of the liquid plus crystal suspensions. As shown in Kolzenburg et al. [2018], crystal growth is progressively limited and potentially impeded in static systems

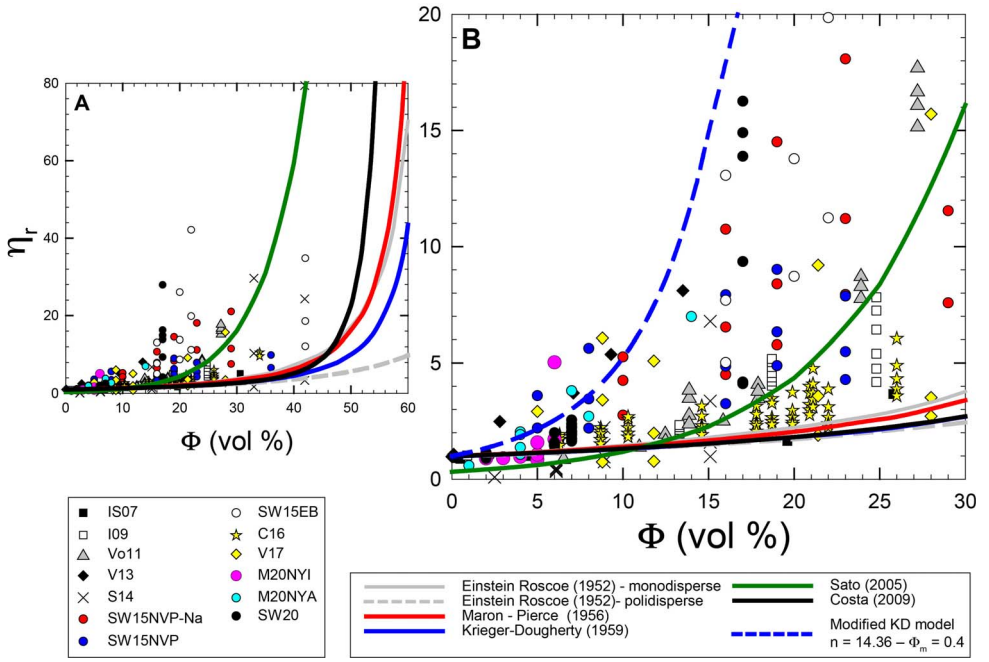

Figure 7. Relative viscosity evolution versus crystal content in vol%. (A, B) reproduce identical dataset with different scale in order to better appreciate difference in relative viscosity induced by different shear rate. Also, note in (B) a modified KD equation [Krieger and Dougherty, 1959] able to reproduce relative viscosity for early departing systems such as those deformed at relatively low shear rate.

(e.g., no shear) because the surrounding (residual intra-crystalline) melt is depleted in the compatible elements (already incorporated by the early growth events) required for further crystal growth. Also, the cooling and the first crystallizing phases enrich the residual and intra-crystalline melts in slow diffusion components (SiO_2 and Al_2O_3), while the drop of temperature determines a progressive slowdown of chemical elements. Dendritic growth is the consequence of such situations, when the movement of chemical species is limited in a solidifying silicate liquid; if the diffusion is so sluggish compared to kinetic condition, nucleation is suppressed and a glass forms [Kirkpatrick, 1981, Lofgren, 1980, Shea and Hammer, 2013, Vetere et al., 2013, 2015]. Shear or any other deformation acting on magmas and silicate liquids enhance the diffusion of elements by mass transfer.

As reported in Kolzenburg et al. [2017], systems cooled in the same thermal range crystallize faster (at low ΔT and high-T) and more abundantly with progressively increasing shear rates. This observation was also reported for isothermal experiments at sub-liquidus conditions by Kouchi et al. [1986], Vona and Romano [2013], Chevrel et al. [2015], and Vetere et al. [2017] and it is now widely accepted that increasing of shear rate increases the crystal growth rate. Also, Vetere et al. [2019, 2020] have shown that the shear rate during cooling influences the growth rate of solid phases. In particular, the growth rate of olivine, in pyroxenite melt at cooling rate of 10 K/h is ca. 5.3×10^{-6} cm/s. Clinopyroxene crystal in shoshonitic melts shows growth rates between 1.2 and 2.1×10^{-6} cm/s as cooling rates vary from 10 to 100 K/h, respectively, under a deformation rate of 1 s^{-1}.

As shown in a simulation for magmatic conditions [Petrelli et al., 2016], mechanisms invoked as responsible for this fast crystal growth rate could be a continuous "fresh feeding ingredient" on individual crystal surfaces. The fast stirring also enhances the formation of new crystal nuclei, as suggested by Emerson [1926], Cashman et al. [1999], and Vona and Romano [2013]. Finally, oxygen fugacity also plays an important role on crystallization processes and related rheological changes [Kolzenburg et al., 2020]. For example, increasing of fO_2 in magmas reaching

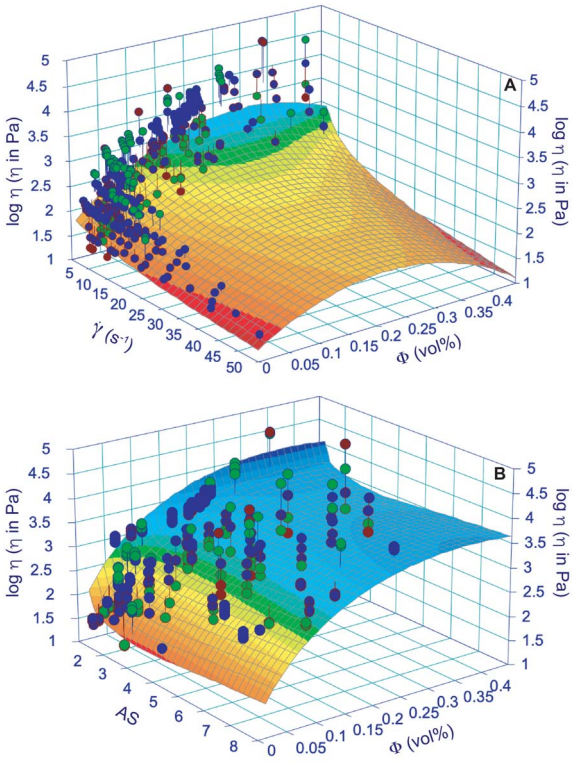

Figure 8. Surface modeling of apparent viscosity with respect of shear rate (γ in s^{-1}) and crystal content (Φ; A) and aspect ratio (AS) and crystal content (Φ; B). The model is based on 415 experimental data provided in Supplementary Appendix 2 derived from chem composition as in Figure 4 and Supplementary Appendix 1. Polynomial approaches (giving the best results in terms of R^2) are provided in Table 1 together with best fit parameters and R^2.

the Earth's surface can lead to a progressive shift of the equilibrium crystallization temperatures.

An example for the evolution of apparent viscosity with decreasing temperature and concomitant crystallization is given in Figure 10 for three different mafic magmas: pyroxenite, basalt, and shoshonite. Experimental conditions in Figure 10 are identical for pyroxenite and shoshonite (cooling rate of 10 K/h and shear rate of 1 s^{-1}), while for basalt the applied cooling rate is slightly higher (30 K/h) and shear rate slightly lower (0.77 s^{-1}). These differences are somewhat minimal, but in terms of reactivity to the cooling event, pyroxenite is the fastest. The kinks in the evolution of viscosity with temperature decrease are related to the onset of crystallization of mineral phases. Pyroxenite, basalt, and shoshonite compositions (composition reported in Figure 4 and Supplementary Appendix 1) have a liquidus temperature, computed by using alphaMELTS of 1543, 1444, and 1452 K, respectively. Obviously, crystallization occurs very quickly after reaching the liquidus temperature for the pyroxenite. The temperature (and time) interval between liquidus and crystallization temperature is larger for the basalt, and even larger for shoshonite. In structural terms, the chemical variability of silicate liquids might be described by the number of non-bridging oxygens (NBO) per tetrahedrally coordinated cation (T) [Mysen and Richet, 2005]:

$$\frac{\mathrm{NBO}}{\mathrm{T}} = \frac{1}{T} \cdot \sum_{i=1}^{i} n \cdot M_i^{n+}, \tag{6}$$

where T is the total atomic abundance of tetrahedrally coordinated cations, M_i^{n+} is the proportion of network modifying cations, "i", with electrical charge n+ after subtraction of the portion required for charge-balancing trivalent cations on tetravalent sites [Mysen and Richet, 2005]. The resulting NBO/T values are 1.14, 0.66, and 0.36 for pyroxenite, basalt, and shoshonite melts, respectively. This shows that high NBO/T values are related with higher cation mobility favoring fast rearrangement of nuclei in order to achieve the "minimum structural unit" for a further crystal growth [Mysen and Richet, 2005]. The curves in Figure 10 reflect the effect of melt structure on the nucleation and crystal growth delay during cooling, as also reported in Vetere et al. [2015] and Iezzi et al. [2017]. Nevertheless, more data are needed to possibly define a better relation between cooling rate, applied shear stress, crystal growth, and NBO/T in order to model viscosity evolution of crystallizing magmas.

Finally, it has recently become evident that the formation of Fe-oxide nanolites can affect the composition of the residual melt and induce change in crystal nucleation and growth processes and thus, on the magma rheological response [Vetere et al., 2015, Di Genova et al., 2020, and reference therein]. While these phases are too small to be analytically quantified with most of the classical techniques applied to characterize the presented dataset, the potential occurrence of these phases might influence the data in some experimental charges.

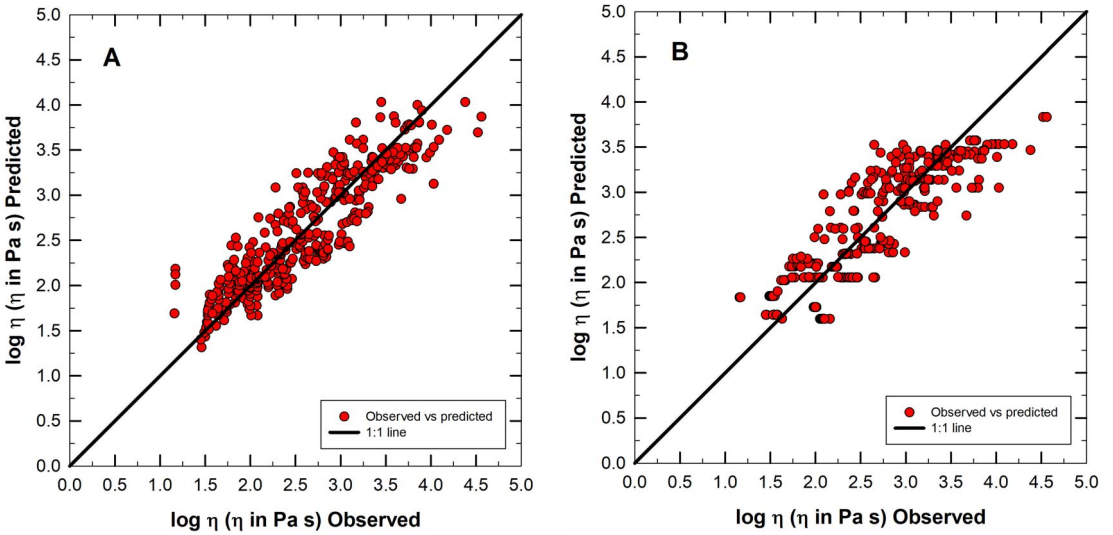

Figure 9. $\log\eta$ observed versus predicted from (4) and (5). (A) refers to (4) with $R^2 = 0.80$ while (B) refers to (5) with $R^2 = 0.75$.

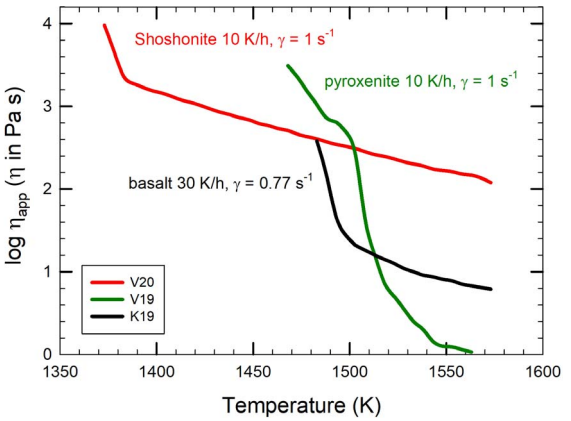

Figure 10. Log apparent viscosity (Pa·s) versus temperature (K) evolution for basaltic, pyroxenite, and shoshonite melt compositions as in Figure 4 and Supplementary Appendix 1. Note the decrease of viscosity as melts cool down and crystallize.

7. Conclusion and future challenges

This review shows that silicate melts subjected to different deformation rates show shear thinning behavior both on pure melts as well as on partly crystallized systems, where crystal content does not exceed ca. 40 vol%. It is obvious that there is still a need for experiments aimed at increasing the available dataset simulating viscosity evolution in crystallizing dynamic systems. Future studies need also to address the effect of pressure, degassing, and related crystallization to expand disequilibrium rheology models to crustal magmatic conditions. A common and rationale strategy is required to study magma rheology by using a common and systematic experimental protocol and this is particularly true for the concentric cylinder approach. From a general point of view, deformation applied to silicate melts enhances nucleation and growth rates of phases when compared to static conditions. This point needs to be considered in modeling magmatic and volcanic behaviors, since rheological behavior could drastically deviate from that predicted based on static experimental approaches and equilibrium modeling.

Conflicts of interest

Authors have no conflict of interest to declare.

Acknowledgements

This study was funded by the "Fondi Ateneo of the University G. D'Annunzio," PRIN (2009PZ47NA_003) project "Experimental determination of the glass-forming ability (GFA), nucleation and crystallization

of natural silicate melts," and PRIN (2017J277S9_003) project "Time scales of solidification in magmas: Application to Volcanic Eruptions, Silicate Melts, Glasses, Glass-Ceramics" awarded to GI. Alexander von Humbold foundation senior research grant to FV is acknowledged.

Supplementary data

Supporting information for this article is available on the journal's website under https://doi.org/10.5802/crgeos.125 or from the author.

References

Applegarth, L. J., Tuffen, H., James, M. R., and Pinkerton, H. (2013). Degassing-driven crystallisation in basalts. *Earth Sci. Rev.*, 116, 1–16.

Armienti, P. (2008). Decryption of igneous rock textures: crystal size distribution tools. *Rev. Mineral.*, 69, 623–649.

Arzi, A. (1978). Critical phenomena in the rheology of partially melted rocks. *Tectonophysics*, 44, 173–184.

Arzilli, F., La Spina, G., Burton, M. R., Polacci, M., Le Gall, N., Hartley, M. E., et al. (2019). Magma fragmentation in highly explosive basaltic eruptions induced by rapid crystallization. *Nat. Geosci.*, 12, 1023–1028.

Asimow, P. D. and Ghiorso, M. S. (1998). Algorithmic modifications extending MELTS to calculate subsolidus phase relations. *Am. Mineral.*, 83, 1127–1132.

Baker, D. R. (2008). The fidelity of melt inclusions as records of melt composition. *Contrib. Miner. Petrol.*, 156, 377–395.

Baker, M. B. and Grove, T. L. (1985). Kinetics controls on pyroxene nucleation and metastable liquid line of descent in a basaltic andesite. *Am. Mineral.*, 70, 279–287.

Campagnola, S., Romano, C., Vona, A., and Giordano, C. G. (2016). Crystallization kinetics and rheology of leucite-bearing tephriphonolite magmas from the Colli Albani volcano (Italy). *Chem. Geol.*, 424, 12–29.

Caricchi, L., Burlini, L., Ulmer, P., Gerya, T., Vassalli, M., and Papale, P. (2007). Non-Newtonian rheology of crystal-bearing magmas and implications for magma ascent dynamics. *Earth Planet Sci. Lett.*, 264, 402–419.

Cashman, K. (1988). Crystallization of Mount-St-Helens 1980–1986 dacite—a quantitative textural approach. *Bull. Volcanol.*, 50, 194–209.

Cashman, K., Thornber, C., and Kauahikaua, J. (1999). Cooling and crystallization of lava in open channels, and the transition of Pahoehoe Lava to "A"(a)over-bar. *Bull. Volcanol.*, 61, 306–323.

Cassidy, M., Manga, M., Cashman, K., and Bachmann, O. (2018). Controls on explosive-effusive volcanic eruption styles. *Nat. Commun.*, 9, article no. 2839.

Chevrel, M. O., Cimarelli, C., deBiasi, L., Hanson, J. B., Lavallée, Y., Arzilli, F., and Dingwell, D. B. (2015). Viscosity measurements of crystallizing andesite from Tungurahua volcano (Ecuador). *Geochem. Geophys. Geosyst.*, 16, 870–889.

Chevrel, M. O., Harris, A. J., James, M. R., Calabrò, L., Gurioli, L., and Pinkerton, H. (2018). The viscosity of pāhoehoe lava: in situ syn-eruptive measurements from Kilauea, Hawaii 2. *Earth Planet. Sci. Lett.*, 493, 161–171.

Chevrel, M. O., Pinkerton, H., and Harris, A. J. L. (2019). Measuring the viscosity of lava in the field: A review. *Earth-Sci. Rev.*, 196, article no. 102852.

Chong, J., Christiansen, E., and Baer, A. (1971). Rheology of concentrated suspensions. *J. Appl. Polym. Sci.*, 15, 2007–2021.

Conte, A. M., Perinelli, C., and Trigila, R. (2006). Cooling kinetics experiments on different Stromboli lavas: Effects on crystal morphologies and phases composition. *J. Volcanol. Geotherm. Res.*, 155(3–4), 179–200.

Cordonnier, B., Hess, K. U., Lavallee, Y., and Dingwell, D. B. (2009). Rheological properties of dome lavas: case study of Unzen volcano. *Earth Planet Sci. Lett.*, 279, 263–272.

Cordonnier, B., Schmalholz, S. M., Hess, K. U., and Dingwell, D. B. (2012). Viscous heating in silicate melts: An experimental and numerical comparison. *J. Geophys. Res.*, 117, article no. B02203.

Costa, A. (2005). Viscosity of high crystal content melts: dependence on solid fraction. *Geophys. Res. Lett.*, 32, article no. L22308.

Costa, A., Caricchi, L., and Bagdassarov, N. (2009). A model for the rheology of particle-bearing suspensions and partially molten rocks. *Geochem. Geophys. Geosyst.*, 10(3), article no. Q03010.

De Paolo, D. J. and Getty, S. R. (1996). Models of isotopic exchange in reactive fluid-rock systems: im-

plications for geochronology in metamorphic rock. *Geochim. Cosmochim. Acta*, 60, 3933–3947.

Del Gaudio, P., Mollo, S., Ventura, G., Iezzi, G., Taddeucci, J., and Cavallo, A. (2010). Cooling rate-induced differentiation in anhydrous and hydrous basalts at 500 MPa: implications for the storage and transport of magmas in dikes. *Chem. Geol.*, 270, 164–178.

Di Genova, D. et al. (2020). In situ observation of nanolite growth in volcanic melt: A driving force for explosive eruptions. *Sci. Adv.*, 6, article no. eabb0413.

Dingwell, D. B. (1995). Viscosity and anelasticity of melts. In *Mineral Physics and Crystallography*, volume 2 of *A Handbook of Physical Constants AGU Reference Shelf*, pages 209–217. American Geophysical Union, Washington.

Dingwell, D. B. (1996). Volcanic dilemma: flow or blow? *Science*, 273, 1054–1055.

Dingwell, D. B. and Webb, S. L. (1989). Structural relaxation in silicate melts and non-Newtonian melts rheology in geologic processes. *Phys. Chem. Miner.*, 16, 508–516.

Dowty, E. (1980). Crystal growth and nucleation theory and the numerical simulation of igneous crystallization. In Hargraves, R. B., editor, *The Physics of Magmatic Processes*, pages 419–485. Princeton University Press, Princeton, NJ, USA.

Eilers, H. (1943). Die viskositäts-konzentrationsabhängigkeit kolloider systeme in organischen lösungsmitteln. *Kolloid-Zeitschrift*, 102, 154–169.

Eilers, V. H. (1941). Die viskosität von emulsionen hochviskoser stoffe als funktion der konzentration. *Kolloid-Zeitschrift*, 97, 313–321.

Einstein, A. (1906). Eine neue Bestimmung der Molekul dimensionen. *Ann. Phys.*, 19, 289–306.

Emerson, O. H. (1926). The formation of aa and pahoehoe. *Am. J. Sci.*, 68, 109–114.

Faroughi, S. A. and Huber, C. (2015). A generalized equation for rheology of emulsions and suspensions of deformable particles subjected to simple shear at low Reynolds number. *Rheol. Acta*, 54, 85–108.

Fiege, A., Vetere, F., Iezzi, G., Simon, A., and Holtz, F. (2015). The roles of decompression rate and volatiles (H_2O + Cl ± CO_2 ± S) on crystallization in (trachy-) basaltic magma. *Chem. Geol.*, 411, 310–322.

Gay, E., Nelson, P., and Armstrong, W. (1969). Flow properties of suspensions with high solids concentration. *AIChE J.*, 15, 815–822.

Ghiorso, M. S., Hirschmann, M. M., Reiners, P. W., and Kress III, V. C. (2002). The pMELTS: A revision of MELTS for improved calculation of phase relations and major element partitioning related to partial melting of the mantle to 3 GPa. *Geochem. Geophys. Geosyst.*, 3(5), 1–36.

Ghiorso, M. S. and Sack, R. O. (1995). Chemical mass transfer in magmatic processes: IV. A revised and internally consistent thermodynamic model for the interpretation and extrapolation of liquid–solid equilibria in magmatic systems at elevated temperatures and pressures. *Contrib. Mineral. Petrol.*, 119, 197–212.

Giordano, D., Russell, J. K., and Dingwell, D. B. (2008). Viscosity of magmatic liquids: a model. *Earth Planet. Sci. Lett.*, 271, 123–134.

Giuliani, L., Iezzi, G., and Mollo, S. (2021). Dynamics of volcanic systems: physical and chemical models applied to equilibrium versus disequilibrium solidification of magmas. In Vetere, F., editor, *Dynamic Magma Evolution*, volume 254 of *American Geophysical Union, Geophysical Monograph*, pages 101–132. John Wiley & Sons, Inc., Hoboken, NJ, USA.

Giuliani, L., Iezzi, G., Tyler, H., Davis, M., Elbrecht, A., Vetere, F., Nazzari, M., and Mollo, S. (2020a). The onset and solidification path of a MORB by in-situ (DSC) and ex-situ investigations. *Front. Earth Sci.*, 8, article no. 337.

Giuliani, L., Iezzi, G., Vetere, F., Behrens, H., Mollo, S., Cauti, F., Ventura, G., and Scarlato, P. (2020b). Evolution of textures, crystal size distributions and growth rates of plagioclase, clinopyroxene and spinel solidified at variable cooling rates from a mid-ocean ridge basaltic liquid. *Earth Sci. Rev.*, 204, article no. 103165.

Giuliani, L., Vetere, F., Iezzi, G., Nazzari, M., Mollo, S., Behrens, H., Scarlato, P., and Ventura, G. (2022). Crystal-chemical variations of spinel, clinopyroxene, and plagioclase in MORB basaltic melt induced by continuous cooling. *Chem. Geol.*, 594, article no. 120765.

Gonnermann, H. M. and Manga, M. (2007). The fluid mechanics inside a volcano. *Annu. Rev. Fluid Mech.*, 39, 321–356.

Guth, E. and Gold, O. (1938). Viscosity and electrovis-

cous effect of the AgI sol. II. Influence of the concentration of AgI and of electrolyte on the viscosity. *Phys. Rev.*, 53, 322.

Hammer, J. E. (2006). Influence of fO_2 and cooling rate on the kinetics and energetics of Fe-rich basalt crystallization. *Earth Planet. Sci. Lett.*, 248, 618–637.

Hammer, J. E. (2008). Experimental studies of the kinetics and energetics of magma crystallization. *Rev. Mineral. Geochem.*, 69(1), 9–59.

Hammer, J. E. and Rutherford, M. J. (2002). An experimental study of the kinetics of decompression-induced crystallization in silicic melt. *J. Geophys. Res.*, 107(B1), article no. 2021.

Herschel, W. and Bulkley, R. (1926). Konsistenzmessungen von Gummi-Benzollösungen. *Kolloid-Z.*, 39, 291–300. Measurement of consistency as applied to rubber-benzene solutions, Proc. ASTM 82, 1925.

Hess, K. U., Cordonnier, B., Lavallee, Y., and Dingwell, D. B. (2007). High-load, high-temperature deformation apparatus for synthetic and natural silicate melts. *Rev. Sci. Instrum.*, 78(7), article no. 075102.

Higgins, M. D. (2006). *Quantitative Textural Measurements in Igneous and Metamorphic Petrology*. Cambridge University Press, Cambridge.

Hoover, S. R., Cashman, K. V., and Manga, M. (2001). The yield strength of subliquidus basalts—experimental results. *J. Volcanol. Geotherm. Res.*, 107, 1–18.

Hui, H. and Zhang, Y. (2007). Toward a general viscosity equation for natural anhydrous and hydrous silicate melts. *Geochim. Cosmochim. Acta*, 71(2), 403–416.

Iezzi, G., Elbrecht, A. L., Davis, M., Vetere, F., Misiti, V., Mollo, S., and Cavallo, A. (2017). Glass Stability (GS) of chemically complex (natural) sub-alkaline glasses. *J. Non Cryst. Solids*, 477, 21–30.

Iezzi, G., Hammer, J. E., Whittington, A., and Neuville, D. R. (2020). Editorial: research topic crystal nucleation and growth in magmatic suspensions. *Front. Earth Sci.*, 8, article no. 607972.

Iezzi, G., Mollo, S., Torresi, G., Ventura, G., Cavallo, A., and Scarlato, P. (2011). Experimental solidification of an andesitic melt by cooling. *Chem. Geol.*, 283, 261–273.

Iezzi, G., Mollo, S., and Ventura, G. (2009). Solidification behaviour of natural silicate melts and volcanological implications. In Lewis, N. and Moretti, A., editors, *Volcanoes: Formation, Eruptions and Modelling*, pages 127–151. Nova Publishers, New York.

Iezzi, G., Mollo, S., Ventura, G., Cavallo, A., and Romano, C. (2008). Experimental solidification of anhydrous latitic and trachytic melts at different cooling rates: The role of nucleation kinetics. *Chem. Geol.*, 253, 91–101.

Ishibashi, H. (2009). Non-Newtonian behavior of plagioclase-bearing basaltic magma: Subliquidus viscosity measurement of the 1707 basalt of Fuji volcano. *Jpn J. Volcanol. Geotherm. Res.*, 181(1–2), 78–88.

Ishibashi, H. and Sato, H. (2007). Viscosity measurements of subliquidus magmas: Alkali olivine basalt from the Higashi-Matsuura district, Southwest Japan. *J. Volcanol. Geotherm. Res.*, 160(2007), 223–238.

Kerr, R. C. and Lister, J. R. (1991). The effects of shape on crystal settling and on the rheology of magmas. *J. Geol.*, 99, 457–467.

Kirkpatrick, R. J. (1981). Kinetics in crystallization of igneous rocks. *Rev. Mineral. Geochem.*, 8, 321–397.

Kolzenburg, S., Giordano, D., Di Muro, A., and Dingwell, D. B. (2019). Equilibrium viscosity and disequilibrium rheology of high magnesium basalt from Piton de la Fournaise volcano, La Reunion, Indian Ocean, France. *Ann. Geophys.*, 62(2), article no. VO218.

Kolzenburg, S., Giordano, D., Hess, K. U., and Dingwell, D. B. (2018). Shear rate-dependent disequilibrium rheology and dynamics of basalt solidification. *Geophys. Res. Lett.*, 45, 6466–6475.

Kolzenburg, S., Giordano, D., Thordarson, T., Höskuldsson, A., and Dingwell, D. B. (2017). The rheological evolution of the 2014/2015 eruption at Holuhraun, central Iceland. *Bull. Volcanol.*, 79(6), article no. 45.

Kolzenburg, S., Hess, K. U., Berlo, K., and Dingwell, D. B. (2020). Disequilibrium rheology and crystallization kinetics of basalts and implications for the phlegrean volcanic district. *Front. Earth Sci.*, 8, article no. 187.

Kouchi, A., Tsuchiyama, A., and Sunagawa, I. (1986). Effect of stirring on crystallization kinetics of basalt: Texture and element partitioning, Contrib. *Mineral. Petrol.*, 9, 429–438.

Krieger, I. M. and Dougherty, T. J. (1959). A mech-

anism for non-Newtonian flow in suspensions of rigid spheres. *Trans. Soc. Rheol.*, 3, 137–152.

Lanzafame, G., Iezzi, G., Mancini, L., Lezzi, F., Mollo, S., and Ferlito, C. (2017). Solidification and Turbulence (Non-laminar) during magma ascent: Insights from 2D and 3D analyses of bubbles and minerals in an Etnean dyke. *J. Petrol.*, 58(8), 1511–1534.

Lanzafame, G., Mollo, S., Iezzi, G., Ferlito, C., and Ventura, G. (2013). Unravelling the solidification path of a pahoehoe "cicirara" lava from Mount Etna volcano. *Bull. Volcanol.*, 75(4), 1–16.

Lasaga, A. C. (1997). *Kinetic Theory in the Earth Sciences*. Princeton University Press, Princeton, NJ, USA.

Lenk, R. (1967). A generalized flow theory. *J. Appl. Polym. Sci.*, 11, 1033–1042.

Liu, Z., Pandelaers, L., Blanpain, B., and Guo, M. (2017). Viscosity of heterogeneous silicate melts: assessment of the measured data and modeling. *ISIJ Int.*, 57, 1895–1901.

Lofgren, G. (1980). Experimental studies on the dynamic crystallisation of silicate melts. In Hargraves, R. B., editor, *The Physics of Magmatic Processes*, pages 487–551. Princeton University Press, Princeton, NJ, USA.

Mader, H. M., Llewellin, E. W., and Mueller, S. P. (2013). The rheology of two-phase magmas: A review and analysis. *J. Vol. Geotherm. Res.*, 257, 135–158.

Maron, S. H. and Pierce, P. E. (1956). Application of Ree–Eyring generalized flow theory to suspensions of spherical particles. *J. Colloid Sci.*, 11, 80–95.

Mezner, T. G. (2014). *The Rheology Handbook*. Vincentz Network, Hanover, 4th edition.

Moitra, P. and Gonnermann, H. M. (2015). Effects of crystal shape- and size-modality on magma rheology. *Geochem. Geophys. Geosyst.*

Mollo, S., Del Gaudio, P., Ventura, G., Iezzi, G., and Scarlato, P. (2010). Dependence of clinopyroxene composition on cooling rate in basaltic magmas: Implications for thermobarometry. *Lithos*, 118, 302–312.

Mollo, S. and Hammer, J. E. (2017). Dynamic crystallization in magmas. In Heinrich, W. and Abart, R., editors, *Mineral Reaction Kinetics: Microstructures, Textures, Chemical and Isotopic Signatures*, volume 16 of *EMU Notes in Mineralogy*, pages 1–46. European Mineralogical Union and the Mineralogical Society of Great Britain & Ireland, Twickenham.

Mollo, S., Lanzafame, G., Masotta, M., Iezzi, G., Ferlito, C., and Scarlato, P. (2011a). Cooling history of a dike as revealed by mineral chemistry: A case study from Mt. *Etna Volcano. Chem. Geol.*, 283, 261–273.

Mollo, S., Putirka, K., Iezzi, G., Del Gaudio, P., and Scarlato, P. (2011b). Plagioclase-melt (dis)equilibrium due to cooling dynamics: implications for thermometry, barometry and hygrometry. *Lithos*, 125, 221–235.

Morrison, A., Whittington, A., Smets, B., Kervyn, M., and Sehlke, A. (2020). The rheology of crystallizing basaltic lavas from Nyiragongo and Nyamuragira volcanoes. *D.R.C. Volcanica*, 3(1), 1–28.

Mueller, S., Llewellin, E. W., and Mader, H. M. (2010). The rheology of suspensions of solid particles. *Proc. R. Soc. A: Math. Phys. Eng. Sci.*, 466, 1201–1228.

Müller, T., Baumgartner, L. P., Foster, C. T., and Vennemann, T. W. (2004). Metastable prograde mineral reactions in contact aureoles. *Geology*, 32, 821–824.

Mysen, B. and Richet, P. (2005). In *Silicate Glasses and Melts*, volume 10 of *Developments in Geochemistry*, pages 291–327. Elsevier Science, Amsterdam.

Nabelek, P. I. (2007). Fluid evolution and kinetics of metamorphic reactions in calc-silicate contact aureoles from H_2O to CO_2 and back. *Geology*, 35, 927–930.

Perugini, D., Petrelli, M., and Poli, G. (2008). A virtual voyage through 3D structures generated by chaotic mixing of magmas and numerical simulations: a new approach for understanding spatial and temporal complexity of magma dynamics. *Vis. Geosci.*, 13, 1–24.

Petrelli, M., El Omari, K., Le Guer, Y., and Perugini, D. (2016). Effects of chaotic advection on the timescales of cooling and crystallization of magma bodies at mid crustal levels. *Geochem. Geophys. Geosyst.*, 17(2), 425–441.

Petrelli, M., El Omari, K., Spina, L., Le Guer, Y., La Spina, G., and Perugini, D. (2018). Timescales of water accumulation in magmas and implications for short warning times of explosive eruptions. *Nat. Commun.*, 9(1), article no. 770.

Pistone, M., Cordonnier, B., Ulmer, P., and Caricchi, L. (2016). Rheological flow laws for multiphase magmas: An empirical approach. *J. Volcanol. Geotherm. Res.*, 321, 158–170.

Polacci, M., Arzilli, F., La Spina, G., et al. (2018). Crystallisation in basaltic magmas revealed via in situ 4D synchrotron X-ray microtomography. *Sci. Rep.*, 8, article no. 8377.

Pupier, E., Duchene, S., and Toplis, M. J. (2008). Experimental quantification of plagioclase crystal size distribution during cooling of a basaltic liquid. *Contrib. Mineral. Petrol.*, 155(5), 555–570.

Putirka, K. D. (2008). Thermometers and barometers for volcanic systems. In *Reviews in Mineralogy and Geochemistry*, volume 69, pages 61–120. Mineralogical Society of America, Virginia, USA.

Roscoe, R. (1952). The viscosity of suspensions of rigid spheres. *J. Appl. Phys.*, 2, 267–269.

Roselle, G. T., Baumgartner, L. P., and Chapman, J. A. (1997). Nucleation-dominated crystallization of forsterite in the Ubehebe peak contact aureole, California. *Geology*, 25, 823–826.

Rosenberg, C. L. and Handy, M. R. (2005). Experimental deformation of partially melted granite revisited: Implication for the continental crust. *J. Metamorph. Geol.*, 23, 19–28.

Rossi, S., M Petrelli, M., Morgavi, D., Vetere, F., Almeev, R., Astbury, R., and Perugini, D. (2019). The role of magma mixing on pre-eruptive dynamics at the Aeolian Islands (Southern Tyrrhenian Sea, Italy). *Lithos*, 324–325, 165–179.

Rusiecka, M. K., Bilodeau, M., and Baker, D. R. (2020). Quantification of nucleation delay in magmatic systems: experimental and theoretical approach. *Contrib. Mineral. Petrol.*, 175(5), article no. 47.

Saar, M. O., Manga, M., Cashman, K. V., and Fremouw, S. (2001). Numerical models of the onset of yield strength in crystal–melt suspensions. *Earth Planet. Sci. Lett.*, 187, 367–379.

Sehlke, A. and Whittington, A. G. (2015). Rheology of lava flows on Mercury: An analog experimental study. *J. Geophys. Res.: Planets*, 120, 1924–1955.

Sehlke, A. and Whittington, A. G. (2020). Rheology of a KREEP analog magma: xperimental results applied to dike ascent through the lunar crust. *Planet. Space Sci.*, 187(2020), article no. 104941.

Sehlke, A., Whittington, A. G., Robert, B., Harris, A., Gurioli, L., Médard, E., and Sehlke, A. (2014). Pahoehoe to àà transition of Hawaiian lavas: an experimental study. *Bull. Volcanol.*, 76(11), article no. 876.

Shapiro, A. P. and Probstein, R. F. (1992). Random packings of spheres and fluidity limits of monodisperse and bidisperse suspensions. *Phys. Rev. Lett.*, 68, 1422.

Shea, T. and Hammer, J. E. (2013). Kinetics of cooling- and decompression-induced crystallization in hydrous mafic-intermediate magmas. *J. Vocanol. Geotherm. Res.*, 260, 127–145.

Smith, P. M. and Asimow, P. D. (2005). Adiabat_1ph: A new public front-end to the MELTS, pMELTS, and pHMELTS models. *Geochem. Geophys. Geosyst.*, 6, article no. Q02004.

Swanson, P. D. and Ottino, J. M. (1990). A comparative computational and experimental study of chaotic mixing of viscous fluids. *J. Fluid Mech.*, 213, 227–249.

Swanson, S. E. (1977). Relation of crystal-growth rate to the granitic textures. *Am. Mineral.*, 62, 966–978.

Tripoli, B., Manga, M., Mayeux, J., and Barnard, H. (2019). The effects of deformation on the early kinetics of basaltic magmas. *Front. Earth Sci.*, 7, article no. 250.

Vand, V. (1948). Viscosity of solutions and suspensions. I. Theory. *J. Phys. Chem.*, 52, 277–299.

Vetere, F. and Holtz, F. (2020). Rheological behavior of partly crystallized silicate melts under variable shear rate. In Vetere, F., editor, *Dynamic Magma Evolution*, Geophysical Monograph Series. Wiley, Hoboken, NJ, USA.

Vetere, F., Iezzi, G., Beherens, H., Holtz, F., Ventura, G., Misiti, V., Cavallo, A., Mollo, S., and Dietrich, M. (2015). Glass forming ability and crystallization behaviour of sub-alkaline silicate melts. *Earth-Sci. Rev.*, 150, 25–44.

Vetere, F., Mazzeo, A., Perugini, D., and Holtz, F. (2020). Viscosity behaviour of silicate melts during cooling under variable shear rates. *J. Non-Cryst. Solids*, 533, article no. 119902.

Vetere, F., Murri, M., Alvaro, M., Domeneghetti, M. C., Rossi, S., Pisello, A., Holtz, F., and Perugini, D. (2019). Viscosity of Pyroxenite Melt and its Evolution during Cooling: an experimental approach. *JGR-Planets*, 124, 1451–1469.

Vetere, F., Petrelli, M., Perugini, D., Haselbach, S., Morgavi, D., Pisello, A., Iezzi, G., and Holtz, F. (2021). Rheological evolution of eruptible Basaltic-Andesite Magmas under dynamic conditions: The importance of plagioclase growth rates. *J. Volcanol. Geotherm. Res.*, 420, article no. 107411.

Vetere, F., Rossi, S., Namur, O., Perugini, D., Morgavi, D., Misiti, V., Mancinelli, P., Petrelli, M., and

Pauselli, C. (2017). Experimental constraints on the rheology, eruption and emplacement dynamics of lavas from Mercury Northern Volcanic Plains. *J. Geophys. Res.: Planets*, 122, 1–17.

Vetere, F., Sato, H., Ishibashi, H., De Rosa, R., and Donato, P. (2013). Viscosity changes during crystallization in shoshonitic magma: new insight on the lava flow emplacement. *J. Mineral. Petrol. Sci.*, 108(3), 144–160.

Vona, A. and Romano, C. (2013). The effects of undercooling and deformation rates on the crystallization kinetics of Stromboli and Etna basalts. *Contrib. Mineral. Petrol.*, 166(2), 491–509.

Vona, A., Romano, C., Dingwell, D. B., and Giordano, D. (2011). The rheology of crystal-bearing basaltic magmas from Stromboli and Etna. *Geochim. Cosmochim. Acta*, 75(11), 3214–3236.

Webb, S. L. and Dingwell, D. B. (1990a). Non-newtonian rheology of igneous melts at high stresses and strain rates: experimental results for rhyolite, andesite, basalt, and nephelinite. *J. Geophys. Res.*, 95, 15695–15701.

Webb, S. L. and Dingwell, D. B. (1990b). The onset of non-Newtonian rheology of silicate melts. *Phys. Chem. Minerals*, 17, 125–132.

Wildemuth, C. and Williams, M. (1984). Viscosity of suspensions modeled with a shear-dependent maximum packing fraction. *Rheol. Acta*, 23, 627–635.

Yue, Y. Z. and Bruckner, R. (1996). On the different descriptions of the non-Newtonian viscosity (shear-thinning effect) of glass melts with respect to heat dissipation. *Gerlands Beitr. Geophys.*, 69(6), 179–185.

Zhang, Y. (2008). *Geochemical Kinetics*. Princeton University Press, Princeton, NJ, USA.